SUPPORTING INFORMATION

Quantum Dot Photoactivation of Pt(IV) Anticancer Agents: Evidence of an Electron Transfer Mechanism Driven by Electronic Coupling

Ivan Infante,[a]* Jon M. Azpiroz,[a] Nina Gomez Blanco, [b]Emmanuel Ruggiero,[b] Jesus M. Ugalde,[a] Juan C. Mareque-Rivas,[b,c] Luca Salassa[b]*

[a] KimikaFakultatea, EuskalHerrikoUnibertsitatea and Donostia International Physics Center (DIPC), P.K. 1072 Donostia, Euskadi, Spain
*e-mail: iinfant76@gmail.com

[b] CIC biomaGUNE, PaseoMiramón 182, 20009, Donostia, Euskadi, Spain
*e-mail: lsalassa@cicbiomagune.es

[c] Ikerbasque, Basque Foundation for Science, 48011, Bilbao, Euskadi, Spain

Materials and experimental methods

Details on the synthesis and characterization of the systems modeled here are described elsewhere (C. R. Maldonado *et al.*, *Chem. Commun.*, 2013, **49**, 3985-3987). Light irradiation experiments were performed on **1** in H_2O/D_2O using a LED source (λ_{exc} = 385 nm, 480 nm of 630 nm, Prizmatix, MWLLS-11, *ca.* 40, 24 and 20mW cm^{-2} respectively). The formation of photoproducts was monitored by ^1H NMR at 298 K (Bruker 500 MHz). Cell toxicity studies were performed on the PC3 cell line (human prostate cancer) using the SRB method with a 72 h incubation period.

XPS experiments were performed in a SPECS Sage HR 100 spectrometer with a non-monochromatic X-ray source Aluminum Kα line of 1486.6eV energy, a power applied of 350 W and calibrated using the $3d_{5/2}$ line of Ag with a full width at half maximum (FWHM) of 1.0eV. The selected resolution for the detailed spectra was 5 eV of Pass Energy and 0.15 eV/step. All measurements were made in an ultra high vacuum (UHV) chamber at a pressure below $5 \cdot 10^{-8}$ mbar.

QD-photoluminiscence (λ_{em} = 657 nm, core-shell CdSe/ZnS) quenching by **1** was studied on QD-micellar solutions (100 nM) by adding increasing amounts of the complex (0–500 μM) and measuring the decrease in QD emission (λ_{exc} = 470 nm, Horiba Jobin-Yvon fluorimeter F1-1065). As previously shown by Tseng *et al.* (*J. Am. Chem. Soc.*, 2013, **135**, 3383-3386), the Stern-Volmer and the Langmuir models were employed to elucidate the type of interaction between the QDs and **1**. The Stern-Volmer expression can describe collisional dynamic quenching, while the Langmuir model can account for static quenching due to (partial) adsorption.

Table S1. Selected bond distances (Å) for the X-ray geometry of **1** and its DFT-optimized ground-state geometry using different functionals and basis sets. See Figure S1 (page S9) for atom numbering.

	Pt–O4	**Pt–O9**	**Pt–N14**	**Pt–N18**	**Pt–Cl2**	**Pt–Cl3**
X-ray	**1.992**	**2.008**	**2.050**	**2.066**	**2.311**	**2.319**
Averaged	2.000		2.058		2.315	
B3LYP/LANL2DZ/6-311G**	2.061	2.061	2.081	2.087	2.402	2.413
PBE0/LANL2DZ/6-311G**	2.036	2.036	2.050	2.056	2.368	2.380
LC-wPBE/LANL2DZ/6-311G**	2.014	2.015	2.031	2.038	2.350	2.361
Averaged	2.014 (+0.014)		2.034 (-0.024)		2.355 (+0.040)	
LC-wPBE/LANL2TZ/6-311G**	2.012	2.012	2.040	2.033	2.340	2.329
Averaged	2.012 (+0.012)		2.036 (-0.022)		2.334 (+0.019)	
CAM-B3LYP/LANL2DZ/6-311G**	2.032	2.031	2.061	2.054	2.389	2.377
Averaged	2.031 (+0.031)		2.057 (-0.001)		2.383 (+0.068)	
M06/LANL2DZ/6-311G**	2.055	2.048	2.076	2.084	2.376	2.391
TPSSh/LANL2DZ/6-311G**	2.055	2.054	2.069	2.075	2.382	2.394
wB97XD/LANL2DZ/6-311G**	2.034	2.038	2.067	2.057	2.388	2.375
PBE (gas)/def2-SVP	2.048	2.055	2.101	2.090	2.354	2.339
PBE/def2-SVP	2.052	2.055	2.084	2.076	2.370	2.359
PBE0/def2-SVP	2.014	2.016	2.057	2.049	2.344	2.333
Averaged	2.015 (+0.015)		2.053 (-0.003)		2.338 (+0.023)	
B1LYP/def2-SVP	2.032	2.037	2.107	2.096	2.351	2.338
B972/def2-SVP	2.022	2.027	2.089	2.077	2.334	2.321
M06-2X/def2-SVP	2.008	2.015	2.058	2.053	2.346	2.339
LC-wPBE/def2-SVP	1.997	1.997	2.041	2.033	2.324	2.313
CAM-B3LYP/def2-SVP	2.012	2.013	2.063	2.055	2.346	2.336
Averaged	2.012 (+0.012)		2.059 (+0.001)		2.341 (+0.026)	
PBE/SBKJC/6-311G**	2.079	2.081	2.093	2.087	2.383	2.372
PBE0/SBKJC/6-311G**	2.037	2.039	2.067	2.060	2.355	2.344
B1LYP/SBKJC/6-311G**	2.059	2.061	2.095	2.089	2.388	2.378
B972/SBKJC/6-311G**	2.049	2.049	2.0779	2.071	2.365	2.353
M06-2X/SBKJC/6-311G**	2.030	2.036	2.069	2.064	2.354	2.351
LC-wPBE/SBKJC/6-311G**	2.018	2.020	2.052	2.046	2.332	2.324
Averaged	2.019 (+0.019)		2.049 (-0.009)		2.328 (+0.013)	
CAM-B3LYP/SBKJC/6-311G**	2.035	2.036	2.073	2.066	2.363	2.353
Averaged	2.035 (+0.035)		2.069 (+0.011)		2.368 (+0.053)	

Table S2. Selected TD-DFT singlet-singlet transitions for **1** in H_2O (PCM) calculated at the PBE0/def2-SVP level using the ground-state geometry.

No.	Energy(eV)	Wavelength (nm)	Oscillator Strength	Major contributions
1	3.65	340	0.0008	HOMO→LUMO (14%) HOMO→L+1 (41%)
2	3.76	330	0.0018	H-1→LUMO (12%) HOMO→LUMO (40%) HOMO→L+1 (25%)
3	3.85	322	0.0026	H-5→LUMO (17%) H-2→LUMO (64%)
4	4.06	305	0.0300	H-4→LUMO(36%) HOMO→LUMO(20%)
5	4.10	302	0.0050	H-4→LUMO (16%) H-4→L+1 (38%)
6	4.12	301	0.0006	H-5→LUMO (17%) H-5→L+1 (12%) H-2→L+1 (56%)
7	4.28	290	0.0051	H-5→LUMO (20%) H-3→LUMO (33%) H-2→LUMO (15%) H-2→L+1 (17%)
8	4.33	286	0.0033	H-1→LUMO (22%) H-1→L+1 (46%)
9	4.36	284	0.0072	H-1→LUMO (40%) H-1→L+1 (29%)
10	4.40	282	0.0033	H-5→L+1 (42%) H-3→L+1 (41%)

Table S3. Selected TD-DFT singlet-singlet transitions for **1** in H_2O (PCM) calculated at the CAM-B3LYP/def2-SVP level using the ground-state geometry.

No.	Energy(eV)	Wavelength (nm)	Oscillator Strength	Major contributions
1	3.76	330	0.0007	H-6→L+1 (10%) H-4→LUMO (13%) HOMO→LUMO (10%) HOMO→L+1 (37%)
2	3.86	321	0.0034	H-4→L+1 (12%) HOMO→LUMO (43%) HOMO→L+1 (14%)
3	3.94	315	0.0027	H-5→LUMO (13%) H-3→LUMO (55%) H-2→LUMO (17%)
4	4.26	291	0.0006	H-4→LUMO (57%)
5	4.29	289	0.0040	H-4→L+1 (13%) H-3→L+1 (31%) H-2→LUMO (13%)
6	4.32	287	0.0154	H-5→L+1 (10%) H-4→L+1 (38%)
7	4.58	271	0.0070	H-3→L+1 (19%) H-2→LUMO (47%)

Table S4. Selected TD-DFT singlet-triplet transitions for **1** in H_2O (PCM) calculated at the PBE0/def2-SVP level using the lowest-lying triplet geometry. The relative energy of the triplet states with respect to the GS can be calculated adding 1.39 eV. This value was calculated with the ΔSCF method (A. Vlček Jr. and S. Záliš, *Coord. Chem. Rev.*, 2007, **251**, 258) which takes into account the energy difference between the ll-T and GS geometry, both calculated as singlets.

No.	Energy(eV)	Wavelength (nm)	Oscillator Strength	Major contributions
1	0.85	1463	0.0	HOMO→LUMO (96%)
2	1.64	755	0.0	H-2→LUMO (44%) H-1→LUMO (24%)
3	1.86	668	0.0	H-22→LUMO (10%) H-5→LUMO (69%) H-4→LUMO (12%)
4	2.52	491	0.0	H-9→LUMO (32%) H-8→LUMO (17%) H-7→LUMO (15%) H-1→LUMO (13%)
5	2.58	480	0.0	H-3→LUMO (33%) H-2→LUMO (11%) H-1→LUMO (16%)
6	2.66	466	0.0	H-4→LUMO (52%)
7	2.83	437	0.0	H-10→LUMO (15%) H-9→LUMO (26%) H-8→LUMO (33%)
8	2.86	433	0.0	H-6→LUMO (16%) H-3→LUMO (12%) H-2→LUMO (23%) H-1→LUMO (28%)

Table S5. Selected TD-DFT singlet-triplet transitions for **1** in H_2O (PCM) calculated at the CAM-B3LYP/def2-SVP level using the lowest-lying triplet geometry. The relative energy of the triplet states with respect to the GS can be calculated adding 1.35eV. This value was calculated with the ΔSCF method (A. Vlček Jr. and S. Záliš, *Coord. Chem. Rev.*, 2007, **251**, 258) which takes into account the energy difference between the ll-T and GS geometry, both calculated as singlets.

No.	Energy(eV)	Wavelength (nm)	Oscillator Strength	Major contributions
1	0.85	1463	0.0	HOMO→LUMO (96%)
2	1.64	755	0.0	H-2→LUMO (44%) H-1→LUMO (24%)
3	1.86	668	0.0	H-22→LUMO (10%) H-5→LUMO (69%) H-4→LUMO (12%)
4	2.52	491	0.0	H-9→LUMO (32%) H-8→LUMO (17%) H-7→LUMO (15%) H-1→LUMO (13%)
5	2.58	480	0.0	H-3→LUMO (33%) H-2→LUMO (11%) H-1→LUMO (16%)
6	2.66	466	0.0	H-4→LUMO (52%)
7	2.83	437	0.0	H-10→LUMO (15%) H-9→LUMO (26%) H-8→LUMO (33%)
8	2.86	433	0.0	H-6→LUMO (16%) H-3→LUMO (12%) H-2→LUMO (23%) H-1→LUMO (28%)

Table S6. Selected bond distances (Å) for the DFT-optimized ground and lowest-lying triplet state geometry of *cis,cis,trans*-$[Pt(NH_3)_2(Cl)_2(O_2CCH_2CH_2CO_2)_2]^{2-}$ and for the ground-state geometry of *cis,trans*-$[Pt(NH_3)_2(O_2CCH_2CH_2CO_2H)_2(Cl)(H_2O)]^{+}$ (LC-wPBE:LanL2DZ/6-311G**).

	***cis,cis,trans*-$[Pt(NH_3)_2(Cl)_2(O_2CCH_2CH_2CO_2)_2]^{2-}$**					
	Pt–O4	**Pt–O9**	**Pt–N14**	**Pt–N18**	**Pt–Cl2**	**Pt–Cl3**
GS	2.014	2.017	2.025	2.026	2.368	2.367
ll-T	2.013	2.032	2.235	2.046	2.477	2.868
	***cis,trans*-*[Pt*$(NH_3)_2(O_2CCH_2CH_2CO_2H)_2(Cl)(H_2O)]^{+}$**					
	Pt–O4	**Pt–O9**	**Pt–N14**	**Pt–N18**	**Pt–Cl2**	**Pt–OH_2**
GS	2.007	2.006	1.995	2.034	2.348	2.084

Figure S1. Structure of *cis,cis,trans*-[$Pt^{IV}(NH_3)_2(Cl)_2(O_2CCH_2CH_2CO_2H)_2$] (**1**) with atom numbering.

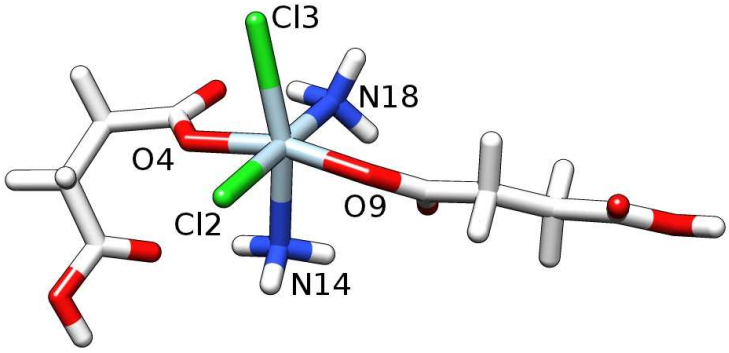

Figure S2. TD-DFT calculated (color) and experimental (black) absorption spectra for **1** in water calculated using the LanL2DZ/6-311G** basis set. The theoretical curves were obtained using GAUSSSUM 2.2 (FWHM = 3000 cm^{-1}) and different functionals.

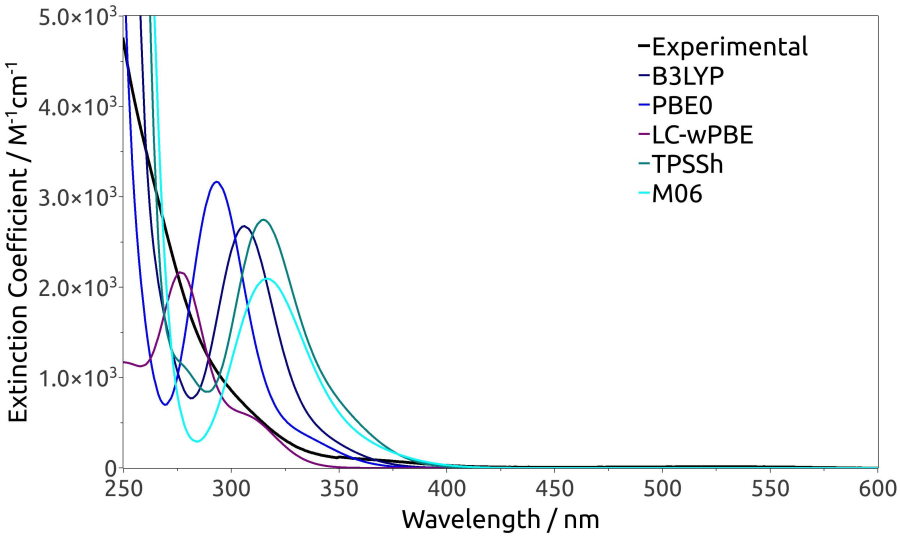

Figure S3. TD-DFT calculated (color) and experimental (black) absorption spectra for **1** in water calculated using the def2-SVP basis set. The theoretical curves were obtained using GAUSSSUM 2.2 (FWHM = 3000 cm^{-1}) and different functionals.

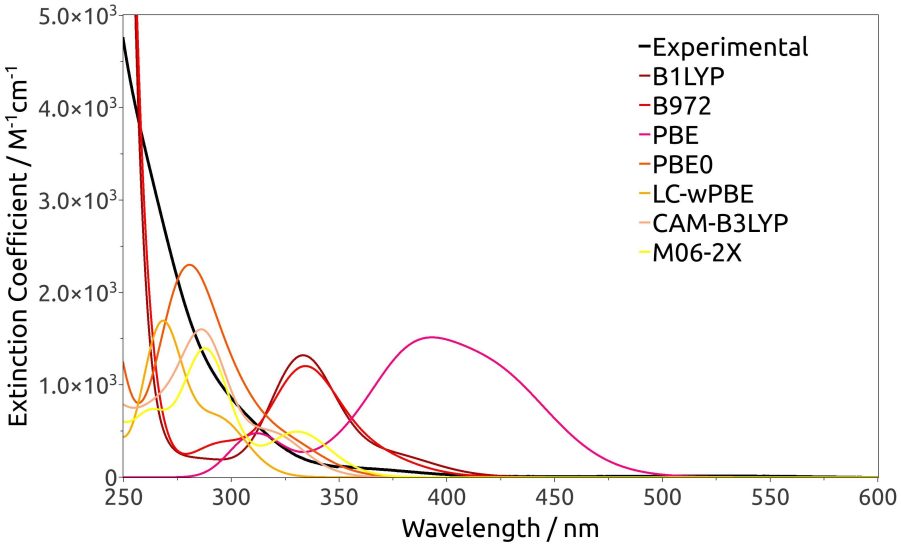

Figure S4. TD-DFT calculated (color) and experimental (black) absorption spectra for **1** in water calculated using the SBKJC/6-311G** basis set. The theoretical curves were obtained using GAUSSSUM 2.2 (FWHM = 3000 cm^{-1}) and different functionals.

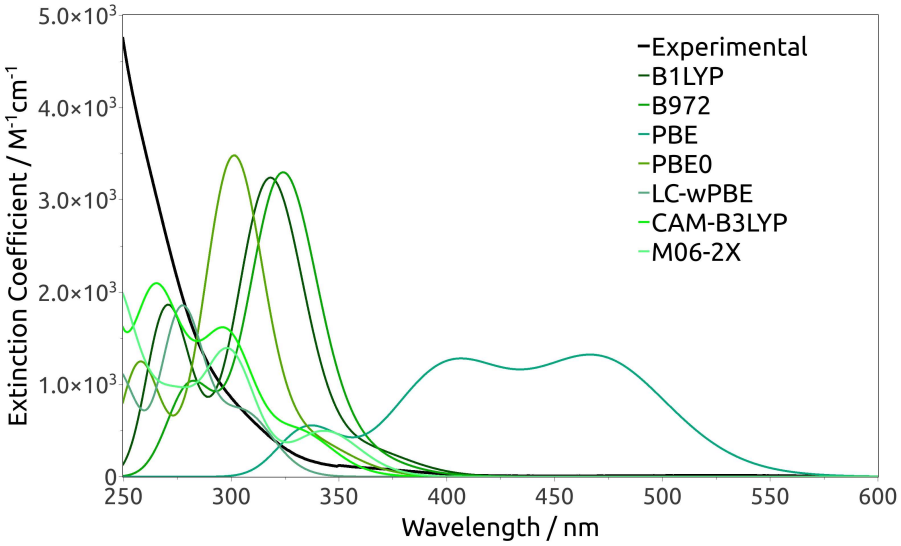

Figure S5. Selected TD-DFT calculated (color) and experimental (black) absorption spectra for **1** in water calculated using different functionals and basis sets. The theoretical curves were obtained using GAUSSSUM 2.2 (FWHM = 3000 cm^{-1}) and different functionals.

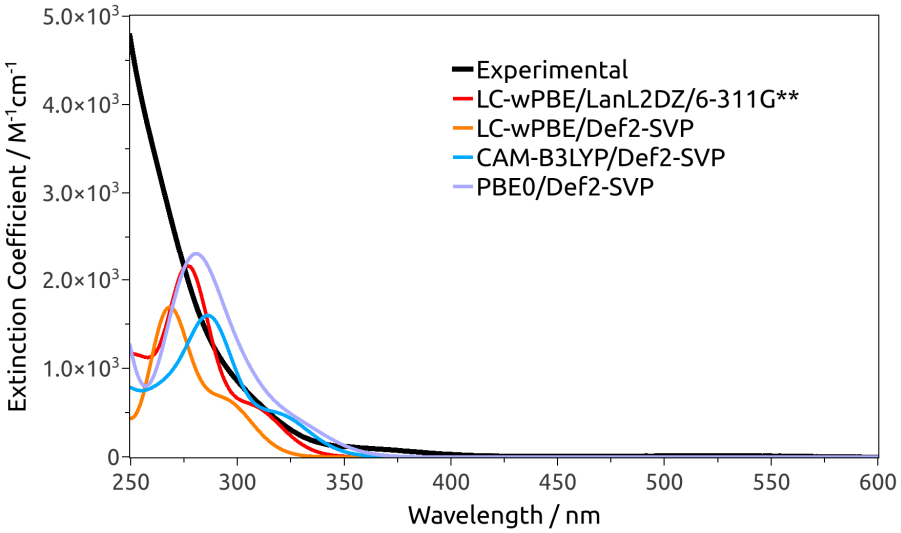

Figure S6. Selected Electron Difference Density Maps (EDDMS) of singlet-singlet electronic transitions for **1** in H_2O (PCM) calculated at the PBE0/def2-SVP level using the ground-state geometry. Violet indicates a decrease in electron density, while purple indicates an increase.

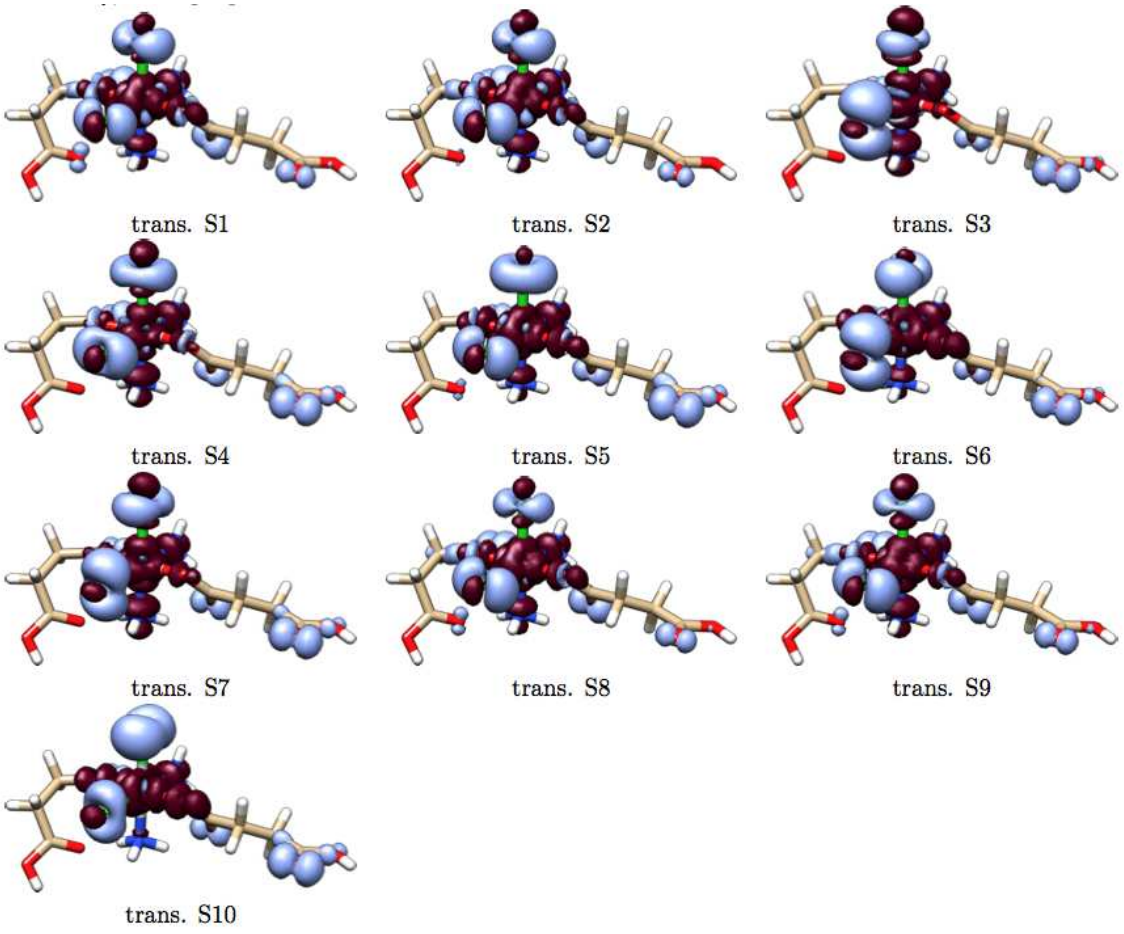

Figure S7. Selected molecular orbitals for **1** calculated at the CAM-B3LYP/def2-SVP level in H_2O (PCM).

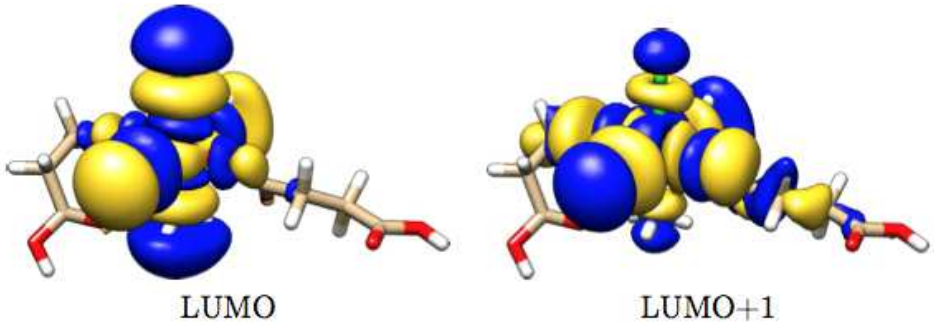

Figure S8. Selected Electron Difference Density Maps (EDDMS) of singlet-singlet electronic transitions for **1** in H_2O (PCM) calculated at the CAM-B3LYP/def2-SVP level using the ground-state geometry. Violet indicates a decrease in electron density, while purple indicates an increase.

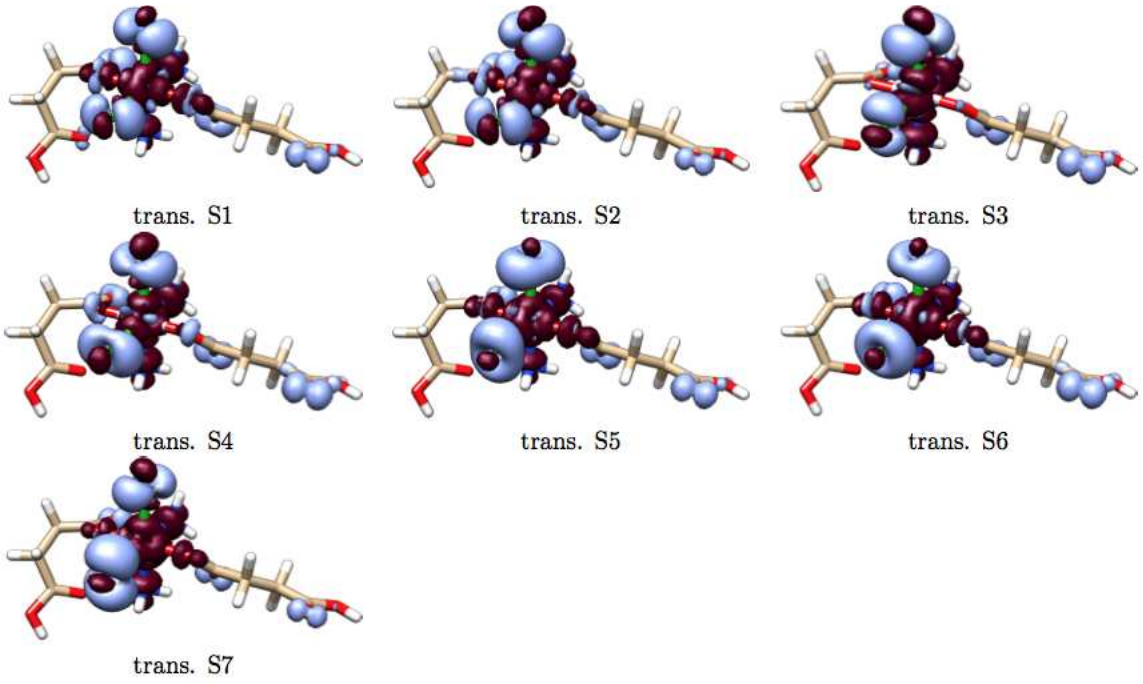

Figure S9. Selected Electron Difference Density Maps (EDDMS) of singlet-triplet electronic transitions and spin density surface for **1** in H_2O (PCM) calculated at the PBE0/def2-SVP level using the ll-T geometry. For EDDMs green indicates a decrease in electron density, while red indicates an increase.

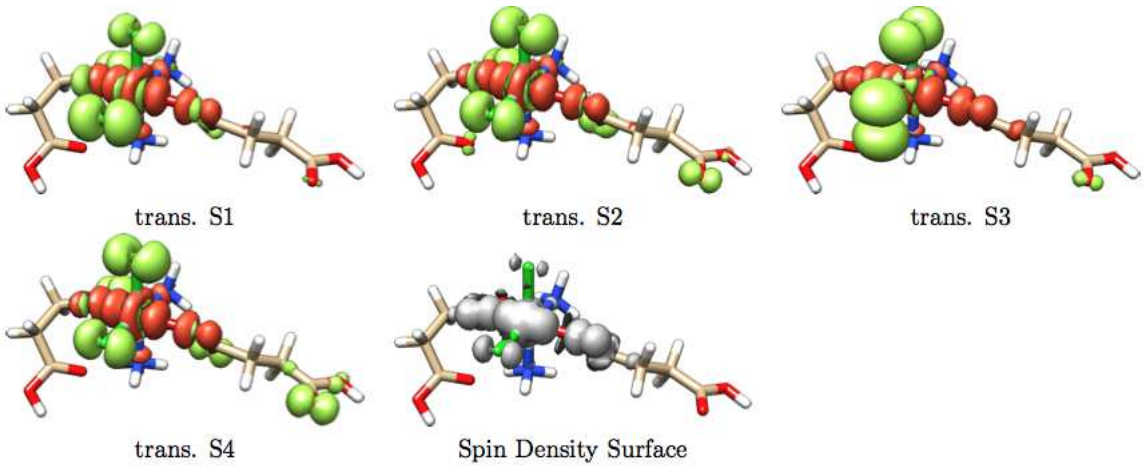

Figure S10. Selected Electron Difference Density Maps (EDDMS) of singlet-triplet electronic transitions and spin density surface for **1** in H_2O (PCM) calculated at the CAM-B3LYP/def2-SVP level using the ll-T geometry. For EDDMs green indicates a decrease in electron density, while red indicates an increase.

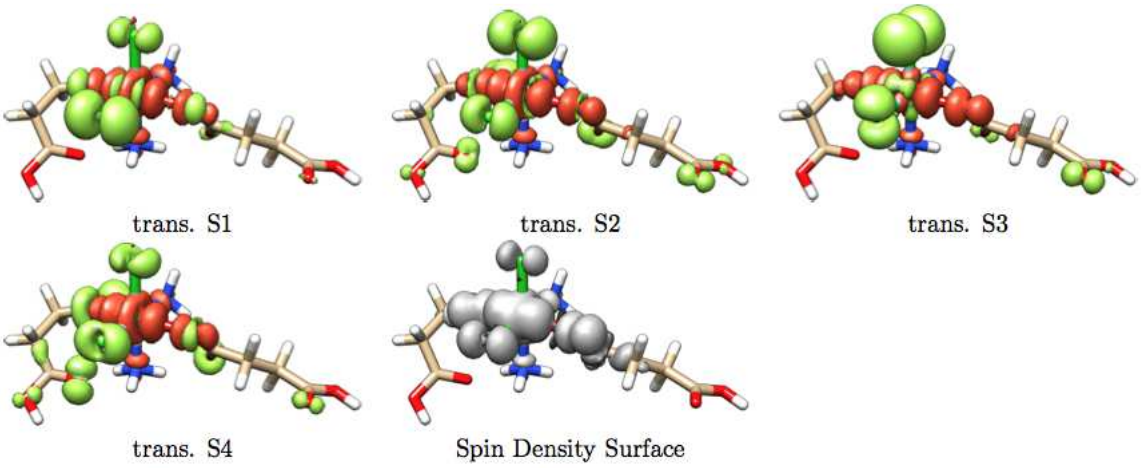

Figure S11. Comparison among the TD-DFT calculated absorption spectra of **1** (black), *cis*,*cis*,*trans*-$[Pt(NH_3)_2(Cl)_2(O_2CCH_2CH_2CO_2)_2]^{2-}$ (blue) and *cis*,*trans*-$[Pt(NH_3)_2(O_2CCH_2CH_2CO_2H)_2(Cl)(H_2O)]^{+}$ (red) in H_2O. The singlet-singlet transitions are shown as vertical bars with heights equal to their oscillator strengths. The theoretical curves were obtained using GAUSSSUM 2.2 and calculation were obtained at the LC-wPBE/LanL2DZ/6-311G** level.

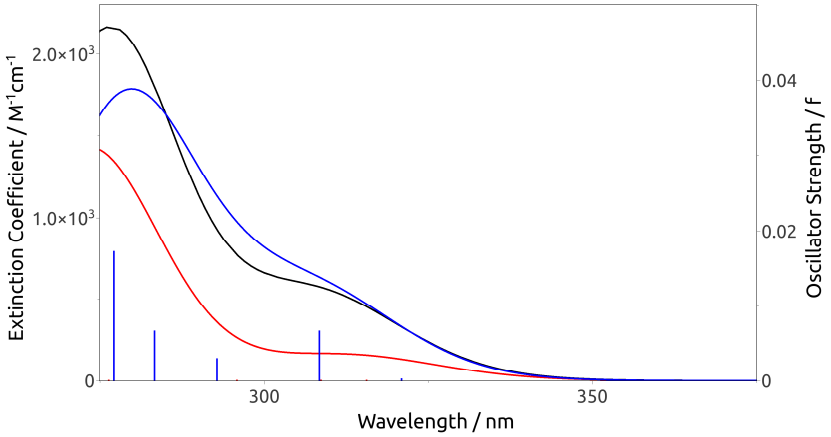

Figure S12. ^{1}H NMR spectrum of **1** in D_2O in the dark and under irradiation with 480-nm and 385-nm light. Generation of free succinic acid (singlet at 2.57 ppm) is obtained only under with UV (385 nm) light (40mW·cm^{-2}).

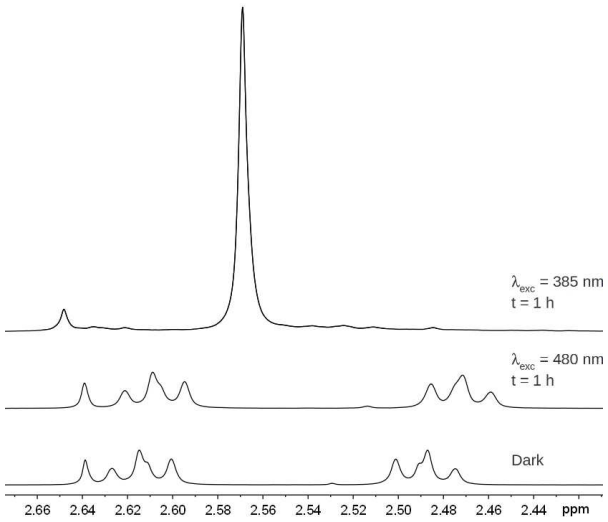

Figure S13. GMP (guanosine 5′-monophosphate) binding experiments on dark and 385-nm irradiated solutions of **1** followed by ^{1}H NMR. Complex **1** was either kept in the dark or irradiated at 385 nm (40mW·cm^{-2}) for 1 h and then incubated in the dark with GMP for 24 h.

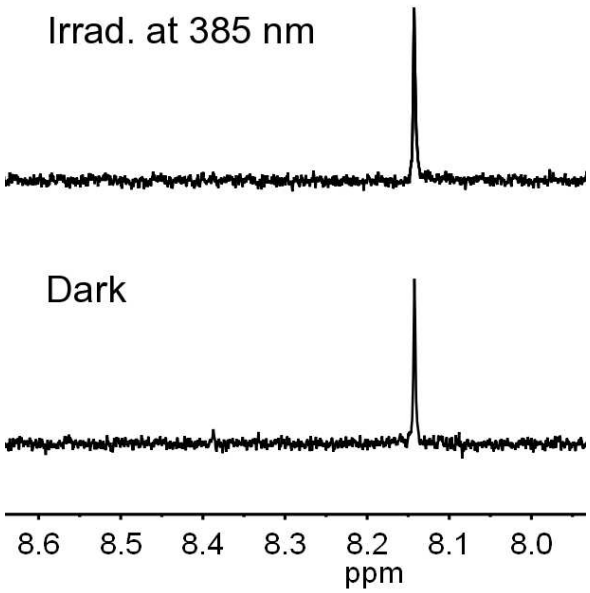

Figure S14. Cell viability studies on the PC3 cell line for solution of **1**(100 μM) preirradiated with 385-nm (40 mW cm^{-2}) and 480-nm (24 mW cm^{-2}) light for 1 h.

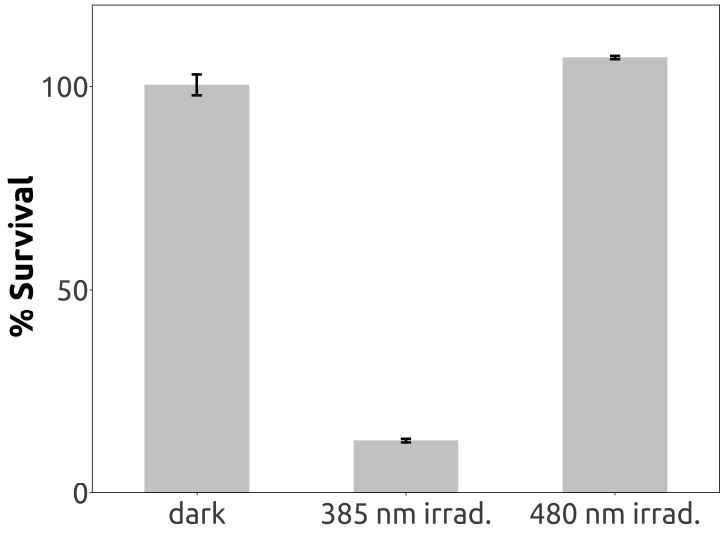

Figure S15. Cell viability studies on the PC3 cell line for solution of *cis,cis,trans*-$[Pt^{IV}(NH_3)_2(Cl)_2(OH)_2]$.

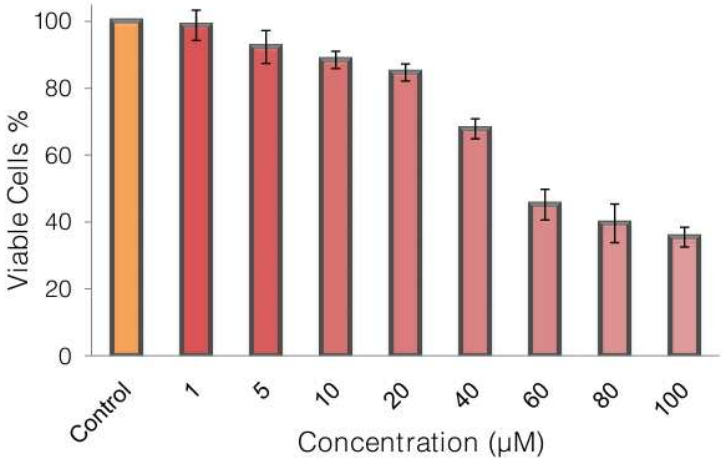

Figure S16. Quenching of QD photoluminescence upon addition of **1** and their fitting to the Langmuir (top) and Stern-Volmer (bottom) models as described in H.-W. Tseng *et al.*, *J. Am. Chem. Soc.* 2013, **135**, 3383.

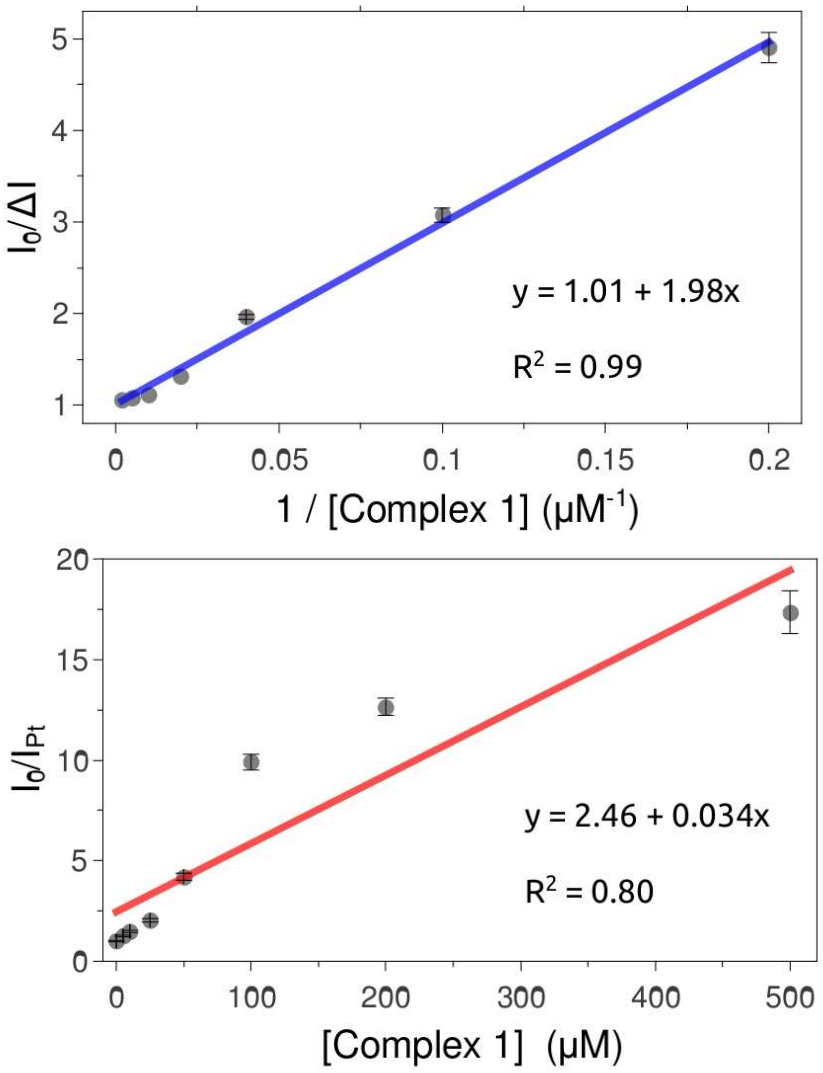

Figure S17. ^{1}H NMR spectrum of **1**(1 mM) in H_2O/D_2O (5:1) in the dark and under irradiation at 630 nm (20 mW·cm^{-2}) in the absence of QD nanocomposites.

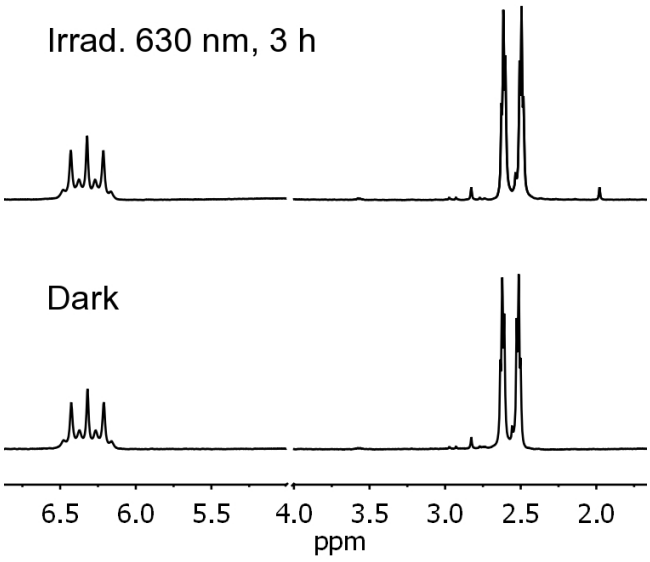

Figure S18. GMP (guanosine 5′-monophosphate) binding experiments on dark and irradiated solutions of **1** followed by ^{1}H NMR. Complex **1** was either kept in the dark or irradiated at 630 nm (20mW·cm^{-2}) in the presence of QD nanocomposites for 3 h and then incubated in the dark with GMP for 24 h.

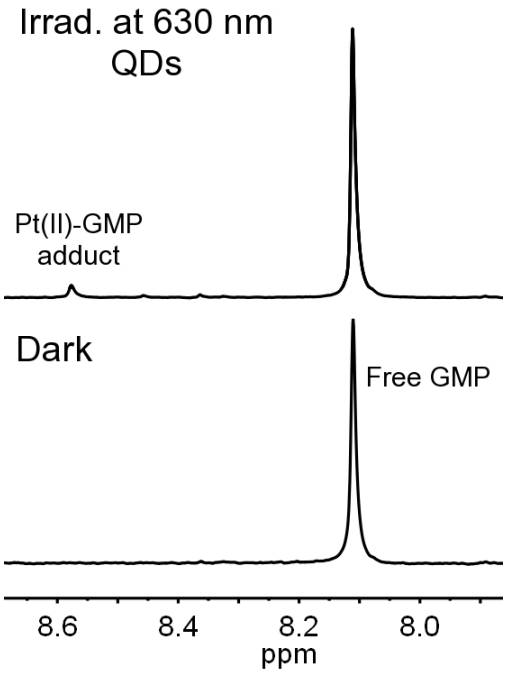

Estimation of the Electron Transfer Kinetics from DFT Calculations

In the following we present the derivation of the equations employed for the estimation of the electron transfer kinetics. As stated in the manuscript, there are two possible ways in which the QD and the Pt complex **1** can interact, via electron energy transfer (EET) or direct electron transfer (ET). In both situations, we assume that the electron donor is always the QD and the acceptor is **1**. EET processes are usually valid within the Dexter (at short-range) and Forster (at long-range) regimes. In these cases, the rate of EET is proportional to the spectral overlap of the donor emission and acceptor absorption spectrum. As inferred by Figure 1 the spectral overlap is negligible, therefore we can rule out the occurrence of EET. The only valid alternative to the reactivity of the QD with **1** is thus the direct ET. The standard theoretical framework for ET processes is the Marcus theory, which in the non-adiabatic and high temperature limits assumes the form:

$$k_{ET} = \sqrt{\frac{\pi}{\hbar \lambda k_b T}} |H_{DA}|^2 exp\left[\frac{-(\Delta G + \lambda)^2}{4\lambda k_b T}\right] (1)$$

where k_b is the Boltzmann constant, T is the temperature, and $\hbar$ is the reduced Planck constant. According to (1), the k_{ET} depends on three tunable variables: (i) the electron coupling term H_{DA}; (ii) the driving force ΔG for the charge separation process, corresponding to the free energy difference between the donor, QD*, and the acceptor **1**; and (iii) the reorganization energyλ, which quantifies the deformation energy of the donor and acceptor upon electron transfer. This latter term is usually decomposed in internal reorganization energy, λ_{INT}, which reflects the response of the molecular donor and acceptor systems to ET and external reorganization energy, λ_{EXT}, associated instead to the rearrangement of the solvent upon ET. Inside the micelle, an excess of organic ligands is present. Assuming this organic shell as a solvent with a very low dielectric, λ_{EXT} is expected to be negligible. The ET activation energy is thus expressed as:

$$\Delta G^{\ddagger} = \frac{(\Delta G + \lambda_{INT})^2}{4\lambda_{INT}} \quad (2)$$

we remind that λ_{INT} and ΔG have opposite sign, which means that the largest ET rate is reached at values of $\Delta G \sim \lambda_{INT}$. For values of $\Delta G < \lambda_{INT}$ the Marcus theory predicts that the

ET rate increases with the driving force, while for $\Delta G > \lambda_{INT}$ a decrease of ET rate occurs at increased driving force (inverted regime).

Internal Reorganization Energy.In the limit of weak interacting fragments, the internal reorganization energy for the charge separation process is defined as:

$$\lambda_{INT} = \lambda_{INT}^{QD^* \rightarrow QD^+} + \lambda_{INT}^{1 \rightarrow 1^-} \quad (3)$$

where$\lambda_{INT}^{QD^* \rightarrow QD^+}$ and $\lambda_{INT}^{1 \rightarrow 1^-}$ are the reorganization energies of the excited QD* and complex **1** during the ET mechanism. Within the framework of density functional theory, these two terms can be computed explicitly as:

$$\lambda_{INT}^{QD^* \rightarrow QD^+} = \frac{\left(E_{(QD^*)}^{QD^*} - E_{(QD^+)}^{QD^*}\right) + \left(E_{(QD^*)}^{QD^+} - E_{(QD^+)}^{QD^+}\right)}{2} = \frac{\lambda_{QD^+}^{QD^*} + \lambda_{QD^*}^{QD^+}}{2} \quad (4)$$

$$\lambda_{INT}^{1 \rightarrow 1^-} = \frac{\left(E_{(1)}^{1} - E_{(1^-)}^{1}\right) + \left(E_{(1)}^{1^-} - E_{(1^-)}^{1^-}\right)}{2} = \frac{\lambda_{1^-}^{1} + \lambda_{1}^{1^-}}{2} \quad (5)$$

the superscript of E indicates the state for which the energy is calculated and the subscript at which equilibrium geometry. In case of direct attachment between the QD and complex **1**, the internal reorganization energy is described as:

$$\lambda_{INT} = \frac{\left(E_{(QD^*-1)}^{QD^*-1} - E_{(QD^+-1^-)}^{QD^*-1}\right) + \left(E_{(QD^*-1)}^{QD^+-1^-} - E_{(QD^+-1^-)}^{QD^+-1^-}\right)}{2} \quad (6)$$

Calculation of this λ_{INT} is a challenging task because it requires computing the relaxed structure of the excited state QD*-**1** complex and of the charge-transfer QD^+-$\mathbf{1}^-$ state. Current TDDFT methodologies suffers for the presence of low-lying charge-transfer transitions that hamper a straightforward localization of the QD*-**1** state. Furthermore, TDDFT also tends to underestimate drastically charge transfer states with errors as high as 1-2 eV. To overcome these technical issues, a simple workaround is to compute the reorganization energies of QD and **1** separately, as in (4) and (5). This approach has been demonstrated to work nicely for several systems (J. Preat, A. Hagfeldt, E. A. Perpète *Energy & Environ. Sci.*, 2011, **4**, 4537). Because we are interested to a qualitative description of the ET mechanism, we believe this is still a good approximation.

Gibbs Free Energy Difference ΔG. In the limit of weak interacting fragments, the Gibbs free energy difference for the charge separation process is computed simply as:

$$\Delta G = -\left[\left(E^{QD^*}_{(QD^*)} + E^{1}_{(1)}\right) - \left(E^{QD^+}_{(QD^+)} + E^{1^-}_{(1^-)}\right)\right] \quad (7)$$

In case of direct attachment, the computation of ΔG for the QD-1 complex is expressed by:

$$\Delta G = -\left(E^{QD^*-1}_{(QD^*-1)} - E^{QD^+-1^-}_{(QD^+-1^-)}\right) \quad (8)$$

With some simple algebraic manipulation, ΔG can thus be computed as:

$$\Delta G = -\left[\left(\omega^{QD-1\rightarrow QD^*-1}_{(QD-1)} - \Delta\omega^{QD^*-1}\right) - \left(\omega^{QD-1\rightarrow QD^+-1^-}_{(QD-1)} - \Delta\omega^{QD^+-1^-}\right)\right] \quad (9)$$

where $\omega^{QD\rightarrow QD^*}_{(QD)}$ is the TDDFT vertical excitation energies of the QD-**1** complex associated to a localized QD* to QD transition. This is computed within a reduced single-excitation subspace to avoid the interference of low-lying charge transfer states. $\omega^{QD\rightarrow QD^*}_{(QD)}$ is the TDDFT vertical excitation energy related to the charge-transfer process, which in this context is usually the first excited state. $\Delta\omega$ refers to the energy difference between the vertical and adiabatic excitation energies of the corresponding excitations. The estimation of these latter two terms is complicated by the knowledge of the relaxed structures of the charge-transfer state and of the excited state. As seen earlier, their evaluation with DFT presents several technical challenges. To overcome these problems, we decided to introduce the following two approximations:

$$\Delta\omega^{QD^*-1} \approx \Delta\omega^{QD^*} = \omega^{QD\rightarrow QD^*}_{QD} - \omega^{QD\rightarrow QD^*}_{QD^*}$$

$$\Delta\omega^{QD^+-1^-} \approx \Delta\omega^{QD^+} + \Delta\omega^{1^-} = \lambda^{QD^+}_{QD} + \lambda^{1^-}_{1}$$

Both approximations imply that the QD*-**1** and QD^+-$\mathbf{1}^-$ excited states of the neutral QD-**1** complex show a structural relaxation equal to the sum of the relaxation of the isolated fragments. This approximation is not always true, however in the cases considered here we assume that it holds because the interaction between the two fragments is never large (at most 2-4 times the magnitude of an hydrogen bond, but still much less than a pure covalent interaction). Finally, the formula to evaluate the ΔG is the following:

$$\Delta G = -\left[\left(\omega^{QD-1\rightarrow QD^*-1}_{(QD-1)} - \lambda^{QD^*}_{QD}\right) - \left(\omega^{QD-1\rightarrow QD^+-1^-}_{(QD-1)} - \left(\lambda^{QD^+}_{QD} + \lambda^{1^-}_{1}\right)\right)\right] \quad (9)$$